

Moreau, K., et al., 2024, Determining the age and origin of a Tertiary karstic system by in situ U-Pb geochronology on speleothems: *Geology*, <https://doi.org/10.1130/G52263.1>

Supplemental Material

Supplemental text, Figures S1 to S15 (field samples, thin-sections, and isochrons), Table S1 (synthesis of U-Pb dating results), and Table S2 (metadata for LA-ICP-MS U-Pb ages of calcite).

METHODS AND MATERIAL STUDIED

Fieldwork, sampling and petrographic work

The carbonate part of the outcrop has been described in detail using the classifications of Dunham (1962) and Embry and Klovan (1971) for textures. The classification by Vennin et al. (2021) is used to describe microbial features in the karst filling. Thin sections were prepared for detailed petrographic observations and *in situ* dating, from the first to the last calcite cement for each cavity. These thin sections were observed under a polarizing optical microscope and observations were completed by cathodoluminescence microscopy, using a cold cathode at 12 kV and 180 μ A coupled to an Olympus BX41 microscope (Olympus Corporation, Tokyo, Japan). After using alizarin-potassium ferricyanide solution, cements were pink-stained suggesting they were non-ferroan calcites. The exact locations of each dated calcite cement are shown on the three schematic sections and thin sections in Figs s1 to s12.

***In situ* U-Pb dating method**

Before U-Pb dating analyses

We adopted the U-Pb dating approach for calcite developed by Roberts et al. (2017) and stated by Brigaud et al. (2021) at the Geoscience Paris-Saclay (GEOPS) laboratory.

A High Resolution Inductively Coupled Plasma Mass Spectrometer (HR-ICP-MS) Element XR (Thermo ScientificTM, Waltham, MA, USA) coupled to a 193 nm ArF Laser Ablation System was used to sample calcite directly on thin sections (TELEDYNE, Thousand Oaks, CA, USA) at the Geosciences Paris-Saclay (GEOPS) laboratory of the University of Paris-Saclay. Previous petrographic work on thin sections under natural light (including stained alizarin-potassium ferricyanide thin sections) and cathodoluminescence enabled us to identify and select 89 calcite cement stages with (1) no evidence of recrystallization, alteration or mixing with detritism, and with (2) 10-15 sparite crystals larger than that of the ablation laser (>160 μ m). These petrographic observations were used to precisely locate the calcite cement stages for each laser ablation spot using Chromium 2.1 software when the sample was placed in the laser ablation system chamber.

Sample selection and reference materials for U-Pb dating

Uranium (^{238}U), lead (^{206}Pb , ^{207}Pb and ^{208}Pb) and thorium (^{232}Th) concentrations were pre-screened by shooting every cement stage five times (89 calcite stages). Most calcite stages (79 out of 89) were suitable for U-Pb dating because (1) uranium concentrations were above 1 ppm (mean of 5.8 ppm), (2) the lead isotopic 206/207 ratio varied, and (3) the U/Pb ratio varied too (allowing us to better constrain the isochron and its intersection with the Concordia).

In situ U-Pb ages were acquired on 43 of the 79 calcite stages presenting high dating potential from 9 thin sections, selected for their interest, such as the first and last cements or the filling sealing. For the U-Pb analysed, glass material NIST614 was used to correct for $^{207}\text{Pb}/^{206}\text{Pb}$ fractionation (Roberts et al., 2017). The laser ablation mass-bias correction of the $^{238}\text{U}/^{206}\text{Pb}$ ratio was corrected using the calcite reference material WC-1 dated by thermal ionization mass spectrometry (TIMS) to 254.4 ± 6.4 Ma (Roberts et al., 2017). Two secondary calcite reference materials were then used to evaluate the accuracy of the U-Pb sessions: (1) Duff Brown Tank (DBT) calcite dated to 64.0 ± 0.7 Ma by U-Pb isotope dilution (Hill et al., 2016) and (2) in-house AUG-B6 calcite, a calcite breccia dated to 43.0 ± 0.7 Ma by LA-ICP-MS (Pagel et al., 2018).

The nine selected thin sections, the three calcite reference materials (WC-1, DBT and the in-house AUG-B6 calcite) and the two glass reference materials (NIST612 (37.38 ppm U and 38.57 ppm Pb) and NIST614 (0.823 ppm U and 2.32 ppm Pb; Jochum et al., 2011)) were all cleaned with pure ethanol and pre-ablated to remove any potential Pb contamination from the surface.

LA-ICP-MS tuning for measurements

The glass reference materials NIST612 and NIST614 were pre-ablated for 3s at a frequency of 10 Hz and a fluence of 6.25 J.cm^{-2} , with laser beam diameters of 50 μm and 135 μm respectively. The samples and calcite reference materials were pre-ablated for 5s at a frequency of 8 Hz and a fluence of 2 J.cm^{-2} with a circular beam of 155 μm . Each analysis consisted of 30s background acquisition followed by 30s of sample ablation and 30s of washout. The glass reference materials NIST612 and NIST614 were ablated at a frequency of 10 Hz and a fluence of 6.25 J.cm^{-2} with a beam size of 40 μm for NIST612 and 110 μm for NIST614. The samples and calcite reference materials were ablated at 8 Hz, a fluence of 1 J.cm^{-2} with a beam

size of 150 μm . The laser-induced aerosol was carried by helium (large volume at 0.5 $\text{l}\cdot\text{min}^{-1}$ and inner cup at around 0.3 $\text{l}\cdot\text{min}^{-1}$) from the sample cell to a mixing funnel in which the sample and He were mixed with 0.950 to 1 $\text{l}\cdot\text{min}^{-1}$ argon and 0.8 to 1.5 $\text{ml}\cdot\text{min}^{-1}$ N_2 to stabilize, amplify and homogenize the aerosol input to the plasma. Signal sensitivity of the ICP-MS was tuned for the best intensity while keeping Th/U between 0.97 and 1.03 and ThO/Th below 0.3 on NIST612. The tuning of the LA-ICP-MS is summarized in Table s2¹. ^{206}Pb , ^{207}Pb , ^{208}Pb , ^{232}Th and ^{238}U isotopes were acquired with integration time per peak (ms) of 10 ms for ^{208}Pb and ^{232}Th , of 20 ms for ^{238}U , of 35 ms for ^{206}Pb and of 45 ms for ^{207}Pb by 750 runs. Measurements were made in fully automated mode overnight in sequences of 398 analyses. One session was performed on 3 September 2021, and two others on 11 and 12 July 2022. Each session began with two NIST612 analyses followed by cycles of one NIST614, one WC-1, one DBT, two AUG-B6, 10 to 15 calcite samples and ended with seven reference material analyses (two AUG-B6, one DBT, one WC-1, one NIST614 and two NIST612). At each stage on calcite samples, a minimum of 10 ablation spots on different crystals was performed on homogenous areas. Ablation spots were located in the middle of the largest calcite crystals to avoid altered areas.

U-Pb ages and uncertainties calculation

Data were processed in Iolite4© using NIST614 as a bracketing primary reference material to correct for baseline subtraction, for Pb isotope mass bias and for $^{206}\text{Pb}/^{238}\text{U}$ instrumental drift over the sequencing time (Paton et al., 2011; Lawson et al., 2018). No down-hole fractionation correction was applied in Iolite© (Nuriel et al., 2017). The two-sigma errors in $^{207}\text{Pb}/^{206}\text{Pb}$ and $^{206}\text{Pb}/^{238}\text{U}$ ratios measured on NIST614 during each analytical session were propagated to the final age uncertainty of calcite samples by quadratic addition (Brigaud et al., 2021). The NIST614 two-sigma errors of the $^{207}\text{Pb}/^{206}\text{Pb}$ varied between 0.33 and 0.47%, while the two-sigma errors of the $^{206}\text{Pb}/^{238}\text{U}$ varied between 1 and 2.5%.

The calcite reference material WC-1 was reduced in a Tera-Wasserburg diagram by using IsoplotR (Vermeesch, 2018) and anchored at 0.85 $^{207}\text{Pb}/^{206}\text{Pb}$ isotopic ratio (Roberts et al., 2017). The ages obtained for the calcite reference materials WC-1, DBT and AUG-B6 and the linear correction factors then applied to correct the $^{206}\text{Pb}/^{238}\text{U}$ ratio and for yielding the correct intercept age (254.4 ± 6.4 Ma; Roberts et al., 2017) are given in Tables s1 and s2¹. The calcite secondary reference material ages during the three sessions for AUG-B6 and for DBT were obtained without fixing the initial $^{207}\text{Pb}/^{206}\text{Pb}$ ratio. Ages obtained on WC-1 were close to the

published age (Roberts et al., 2017), allowing us to use low correction factors between 0.88 and 0.94 for our data. Considering the uncertainties for AUG-B6, the ages are identical with the reference (Pagel et al., 2018). For their part, DBT ages are slightly older than the published age but still within the uncertainties (Hill et al., 2016). Detailed metadata for LA-ICP-MS calcite U-Pb geochronology are available in the Supplementary Data (Table s2¹). Each data item was then plotted in a Tera-Wasserburg diagram using IsoplotR (Vermeesch, 2018) without anchoring the initial $^{207}\text{Pb}/^{206}\text{Pb}$ ratio and using the Discordia model-1. The robust-fit model of Pollard et al (2023) was also tested using the same parameters. Data with uncertainties greater than 50% were considered unusable and were removed from the dataset for the construction of the isochrones (3% of the total data). In each Tera-Wasserburg plot, ages are given with uncertainties related to (1) the decay constant of ^{238}U and ^{235}U , (2) the systematic uncertainty of the age of primary reference material WC-1 (2.6%; Roberts et al., 2017) and (3) the 2-sigma errors of the $^{207}\text{Pb}/^{206}\text{Pb}$ and $^{206}\text{Pb}/^{238}\text{U}$. All Tera-Wasserburg plots are given in Fig s13.

Supplementary discussion about the precision and accuracy of the ages

Since most ages are around 29 Ma and were obtained along 3 different sessions, the ages obtained are probably robust. Woodhead and Petrus (2020) recommended a minimum of 30 ablation shots per stage to form the most robust age and get as close as possible to the ages obtained by the dilution method. In our study, we used only 10 to 16 ablation shots per calcite cement, but by assuming that some stages are contemporary thanks to their close petrographic relationships (then confirmed by their individual U-Pb ages), a single event can be dated with between thirty and one hundred ablation spots (Fig. s14). The new isochrons are still consistent with an average age of 29 Ma.

A majority of the ages have low uncertainty for the method used, between 4% and 8%, including uncertainties down to 3.6%, i.e., absolute uncertainties of 1.0 Ma. The minor uncertainties about ages are because most of the calcite cements analysed have high U contents and high $^{238}\text{U}/^{206}\text{Pb}$ and low $^{207}\text{Pb}/^{206}\text{Pb}$ ratios, placing points near the intersection with the Concordia in the Tera-Wasserburg diagrams. However, rafts completing filling generally have higher uncertainties due to their lower U contents, lower $^{238}\text{U}/^{206}\text{Pb}$ ratios and imprecise $^{207}\text{Pb}/^{206}\text{Pb}$ ratios (Fig. s15). This difference in U and Pb concentrations in the calcite rafts between the base and the top of the fill may result from changes in the chemistry of the meteoric fluid entering the karst, or post-depositional alteration.

It would be difficult to obtain more precise ages since WC-1 calcite is used as a standard for isotope ratio corrections. The age of this calcite has an uncertainty of 2.6%, so it is extrapolated to our data (Roberts et al., 2017). It was, therefore, not considered necessary to multiply the number of analyses per stage in our case and consequently to lengthen the analysis time since the difference in absolute uncertainty between 3.6% and 2.6% is 200 to 300 ka. The precision obtained with the laser ablation method is not as good as with the MC-ICPMS or TIMS dilution methods, which can yield ages with uncertainties of 2–3% or even 1% (Woodhead et al., 2006; Decker et al., 2018). Nevertheless, this method has proved capable of dating calcite stages of 500 μm thick cements using only 10^{-3} mm^3 of calcite for one age, making it very useful for dating stages that are too thin for the dilution method. The laser ablation and dilution methods may even be complementary for dating karst systems, allowing the dating of the most possible stages of speleothems when isotopic conditions are present. To use this *in situ* dating method, we recommend sampling a few grams of calcite to make thin sections or resin plots and carrying out petrographic work before the dating session.

SUPPLEMENTARY FIGURE CAPTIONS

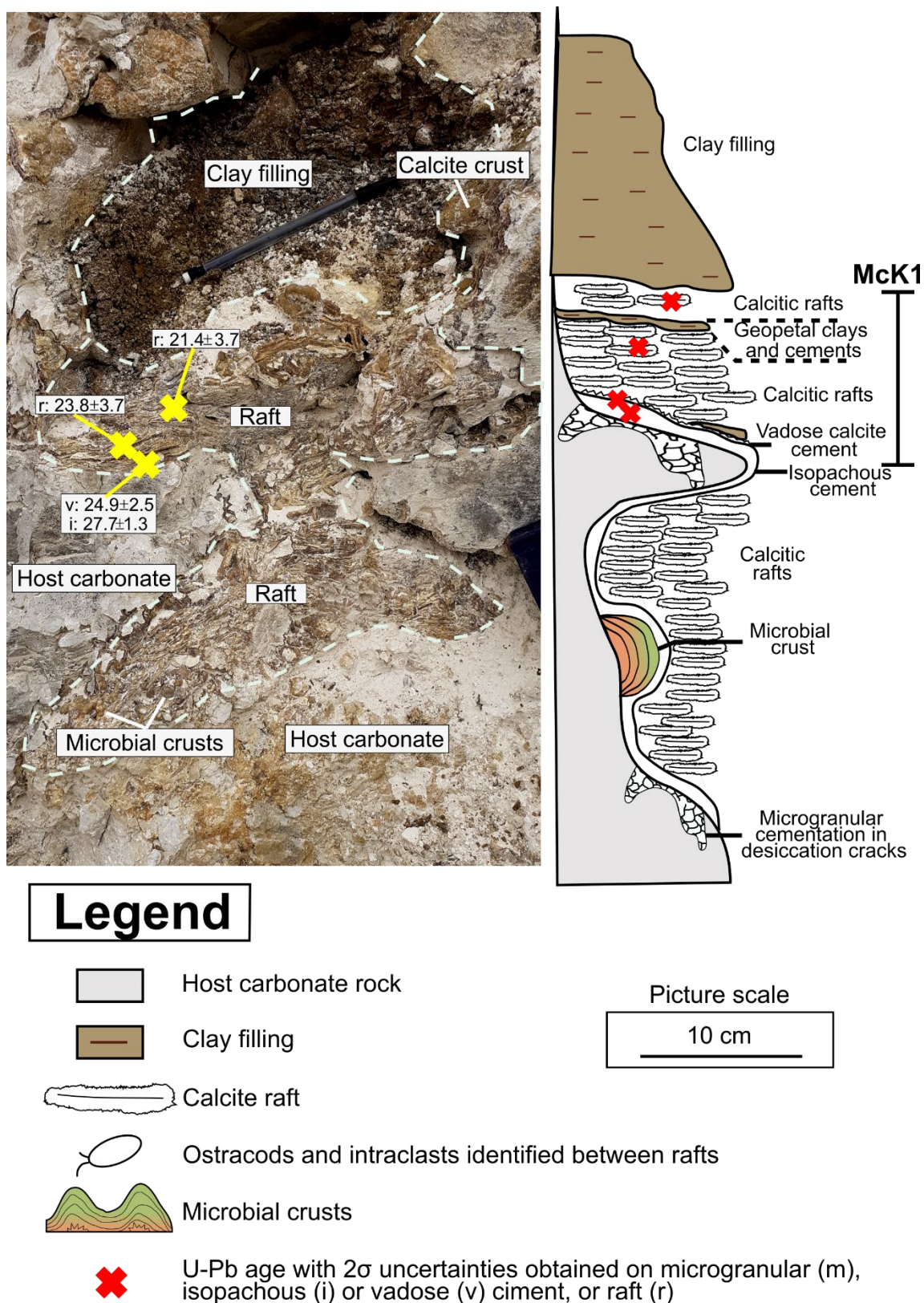


Fig. s1. Photo and schematic sedimentary section of the McK-1 cavity showing the location of the samples collected and of the U-Pb ages obtained by LA-ICP-MS on speleothems.

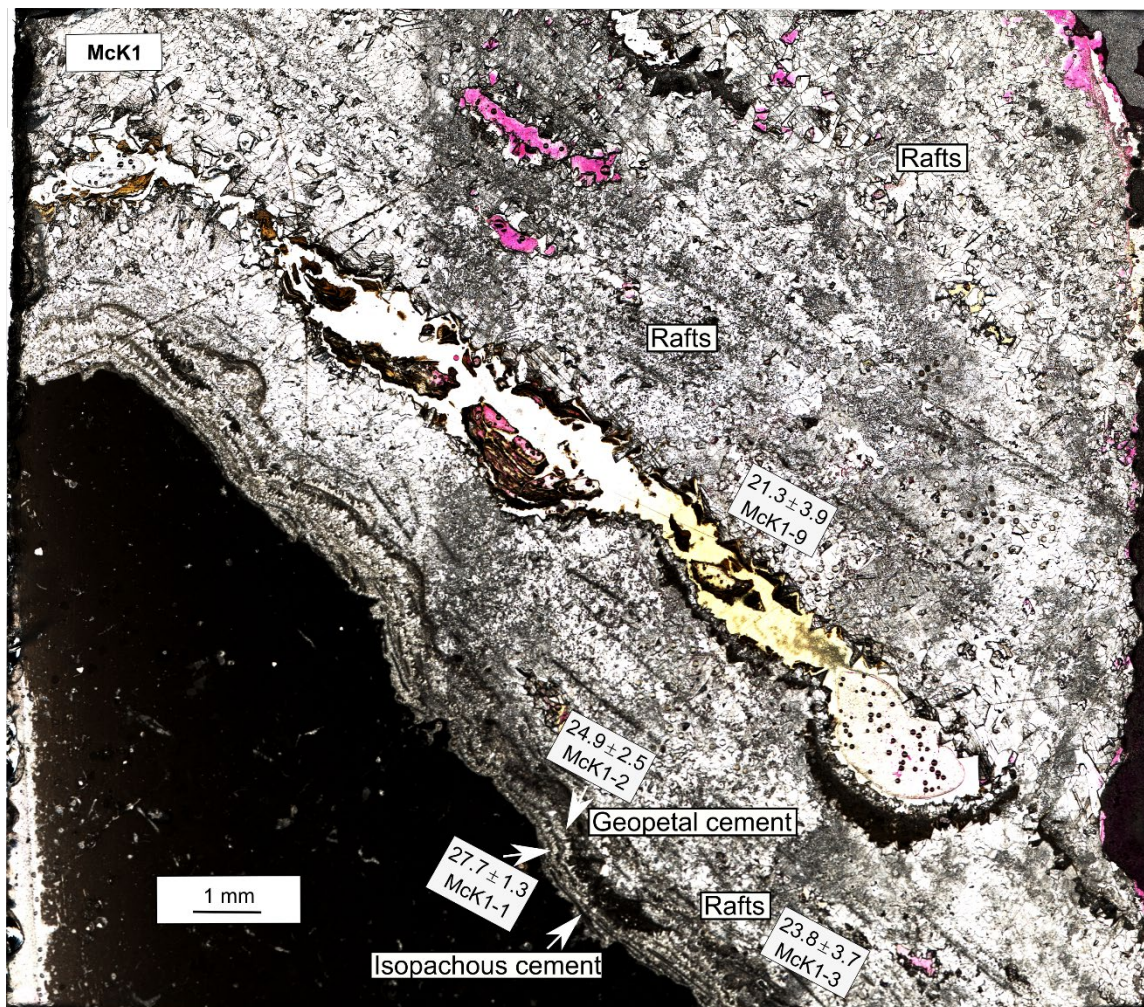


Fig. s2. Thin section (sample McK1-1) with location of U-Pb dated calcite (one isopachous cement, one geopetal cement and two rafts). Pink areas are relics of the treatment with alizarin-potassium ferricyanide solution.

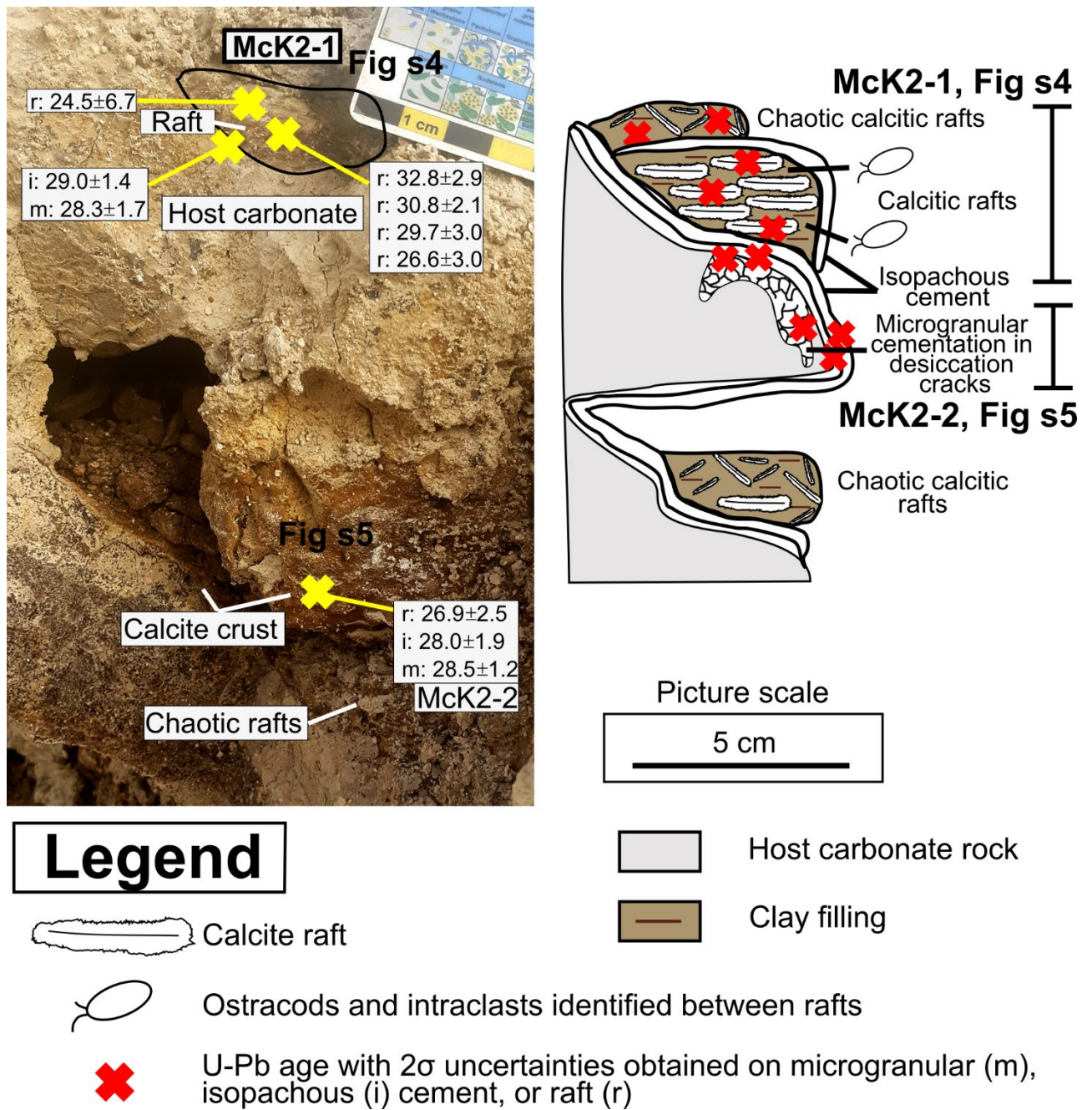


Fig. s3. Photo and schematic sedimentary section of the McK-2 cavity showing the location of the samples collected and of the U-Pb ages obtained by LA-ICP-MS on speleothems.

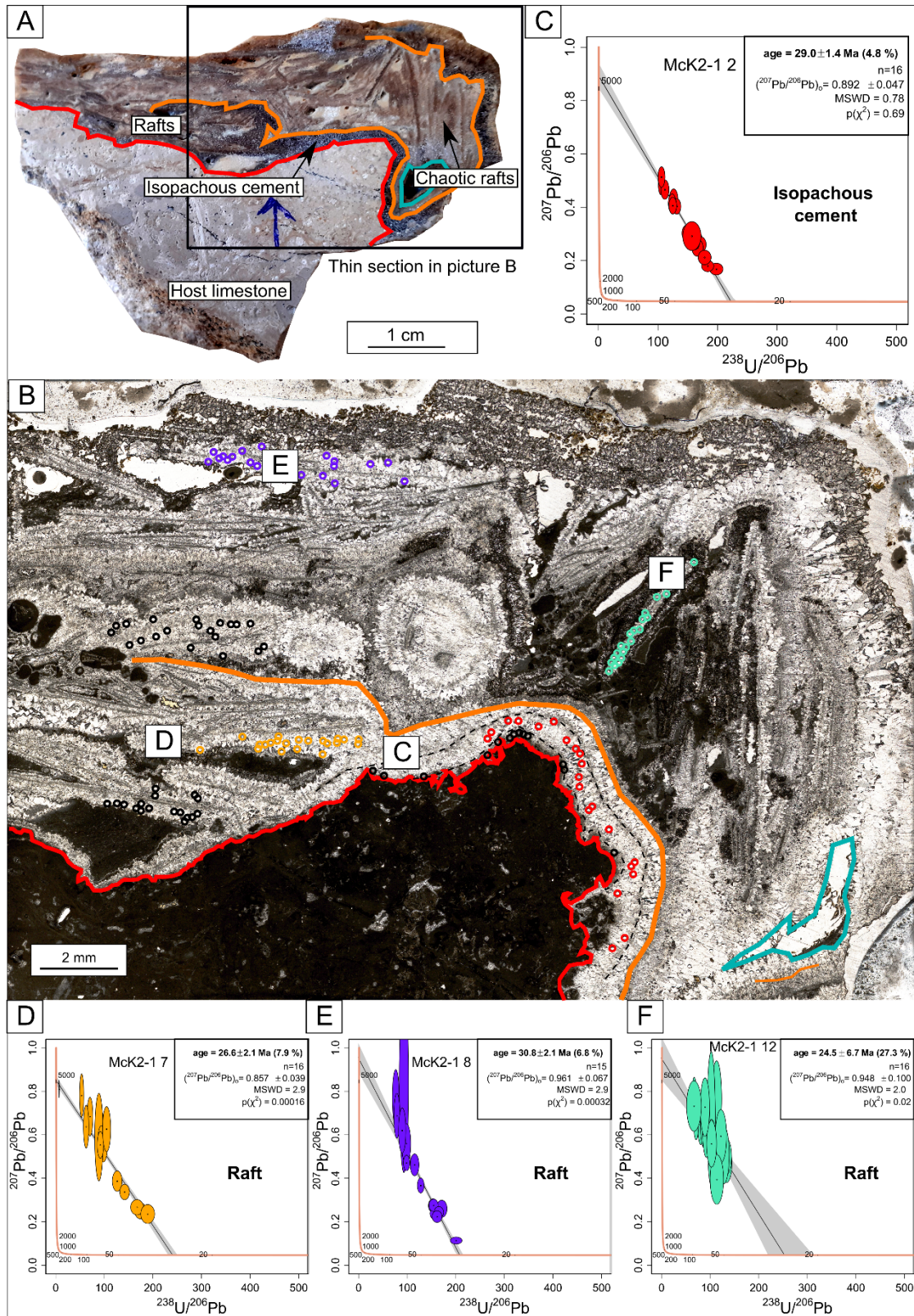


Fig. s4. Detail of McK2-1 sample with the location of U-Pb dated calcite stages. A. McK-2 sample collected in the field (location in Fig. s3). The red line represents the contact between the host carbonate and the first generation of calcite cements; the orange line is the contact between the isopachous cements and horizontally deposited rafts with the second generation of

calcite rafts deposited chaotically; and the blue line delimits a pore space. B. Optical microscopy view of thin-section McK2-1 with the location of U-Pb dating spots in red (first stage of isopachous calcite), orange (raft), purple (raft) and green (raft). C to F. Tera-Wasserburg plot displaying $^{238}\text{U}/^{206}\text{Pb}$ versus $^{207}\text{Pb}/^{206}\text{Pb}$ for each generation of cement. The dated cement generation is located in picture B, in the corresponding colour. Each ellipse represents one laser spot with the analysed uncertainties. The intersection of the isochron (dark line) with the Concordia (orange line) allows us to estimate age. Grey intervals represent the 2σ uncertainty.

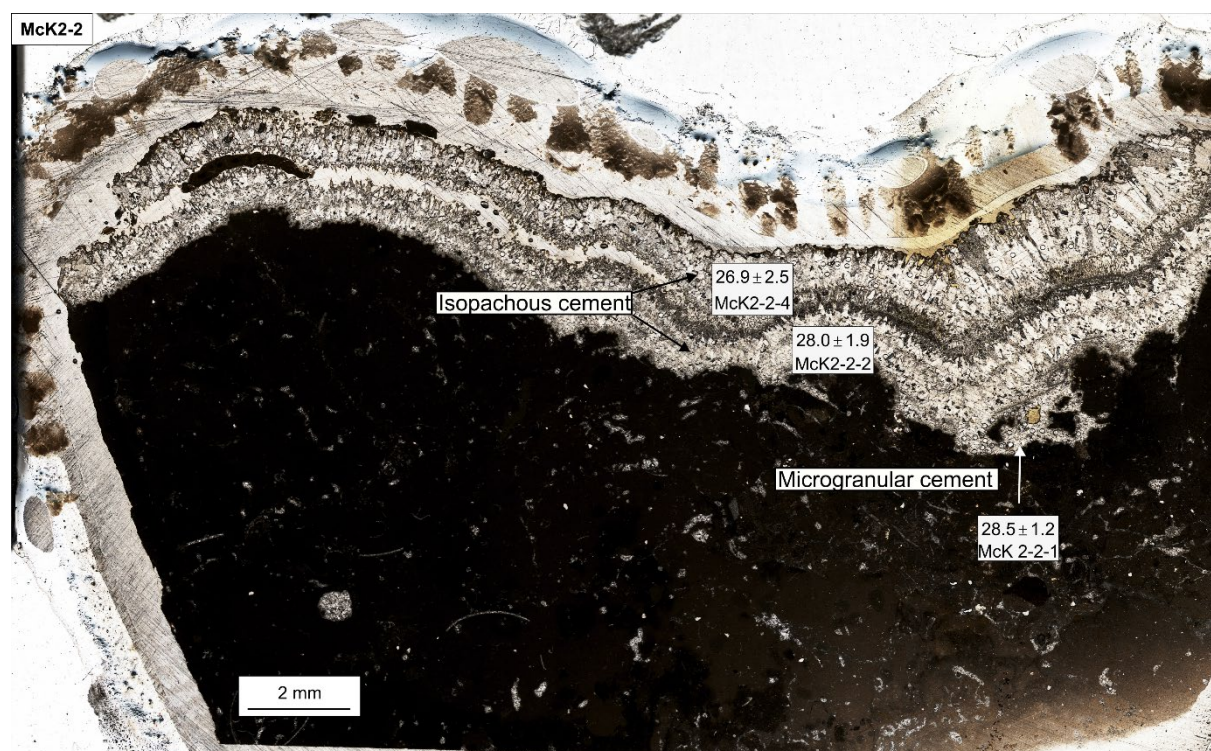


Fig. s5. Thin section of sample McK2-2 with location of U-Pb dated calcite stages (one microgranular calcite cement, two isopachous cements).

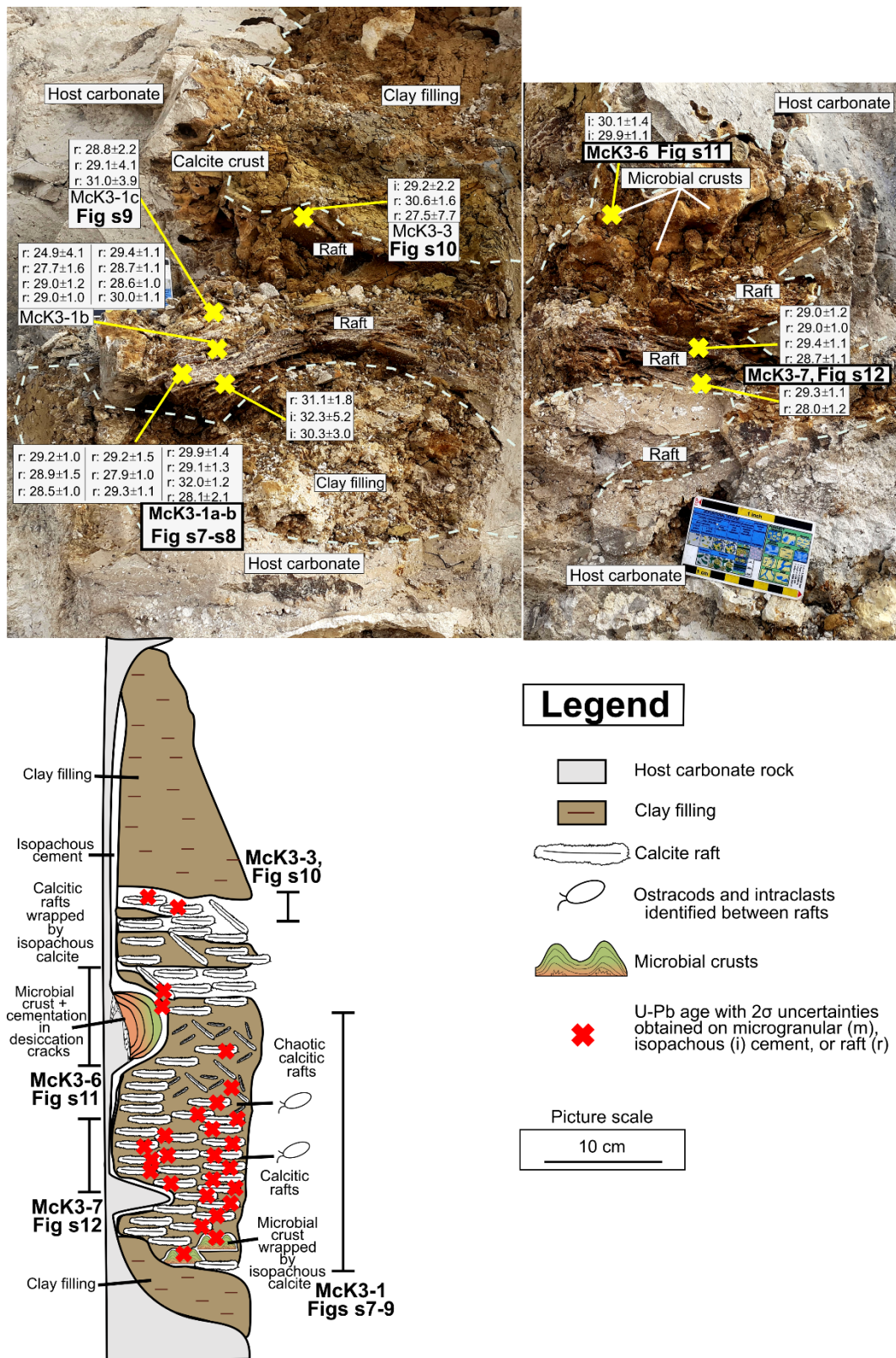


Fig. s6. Photos and schematic sedimentary section of the McK-3 cavity showing the location of the samples collected and the U-Pb ages obtained by LA-ICP-MS on the various calcite cements.



Fig. s7. Thin section of sample McK3-1a with location of U-Pb dated calcite stages (two isopachous cements; McK3-1a2 and 4; six rafts; McK3-1a5 to 10).



Fig. s8. Thin section of sample McK3-1b with location of U-Pb dated calcite stages (seven rafts).

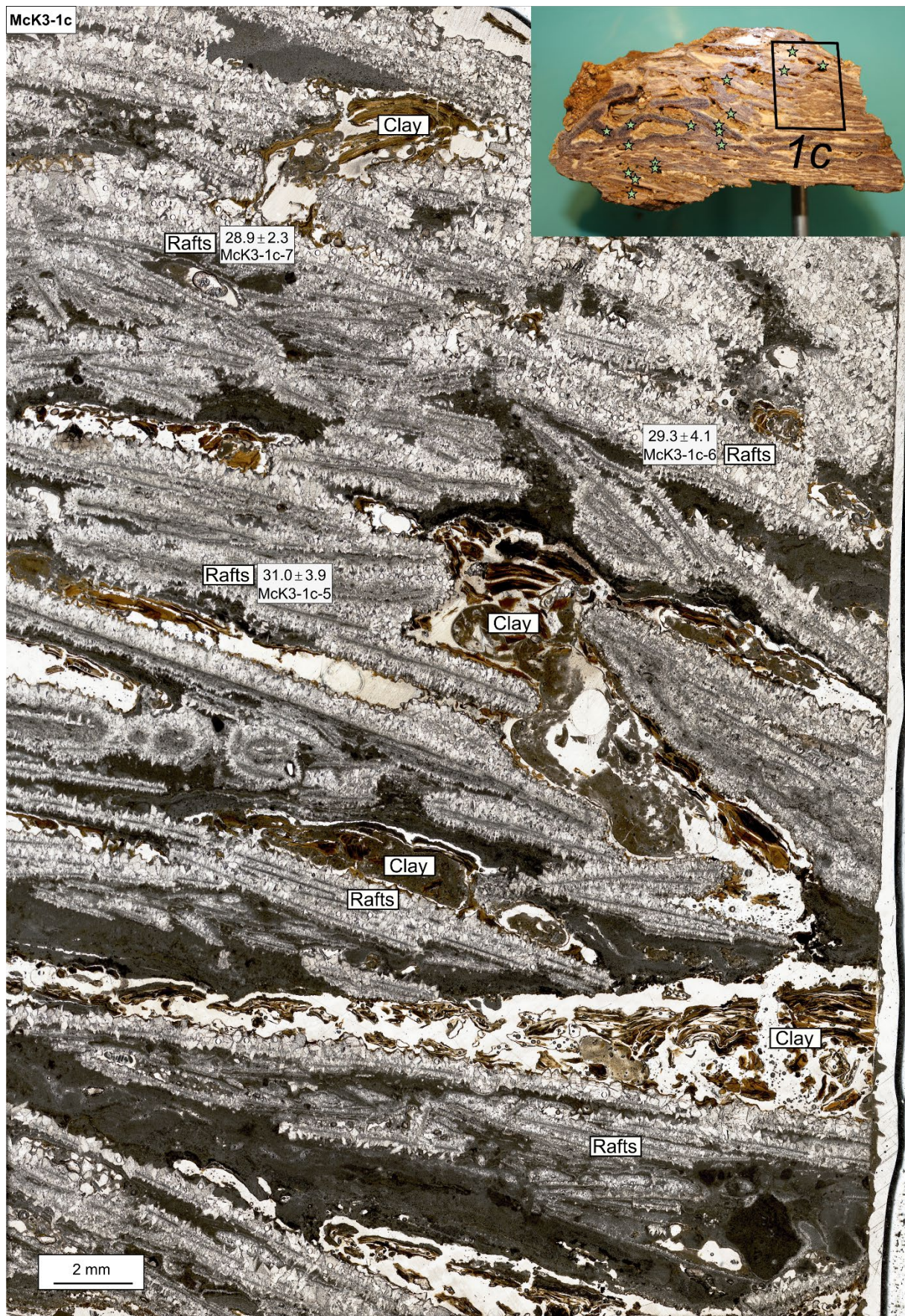


Fig. s9. Thin section of sample McK3-1c with location of U-Pb dated calcite stages (three rafts).

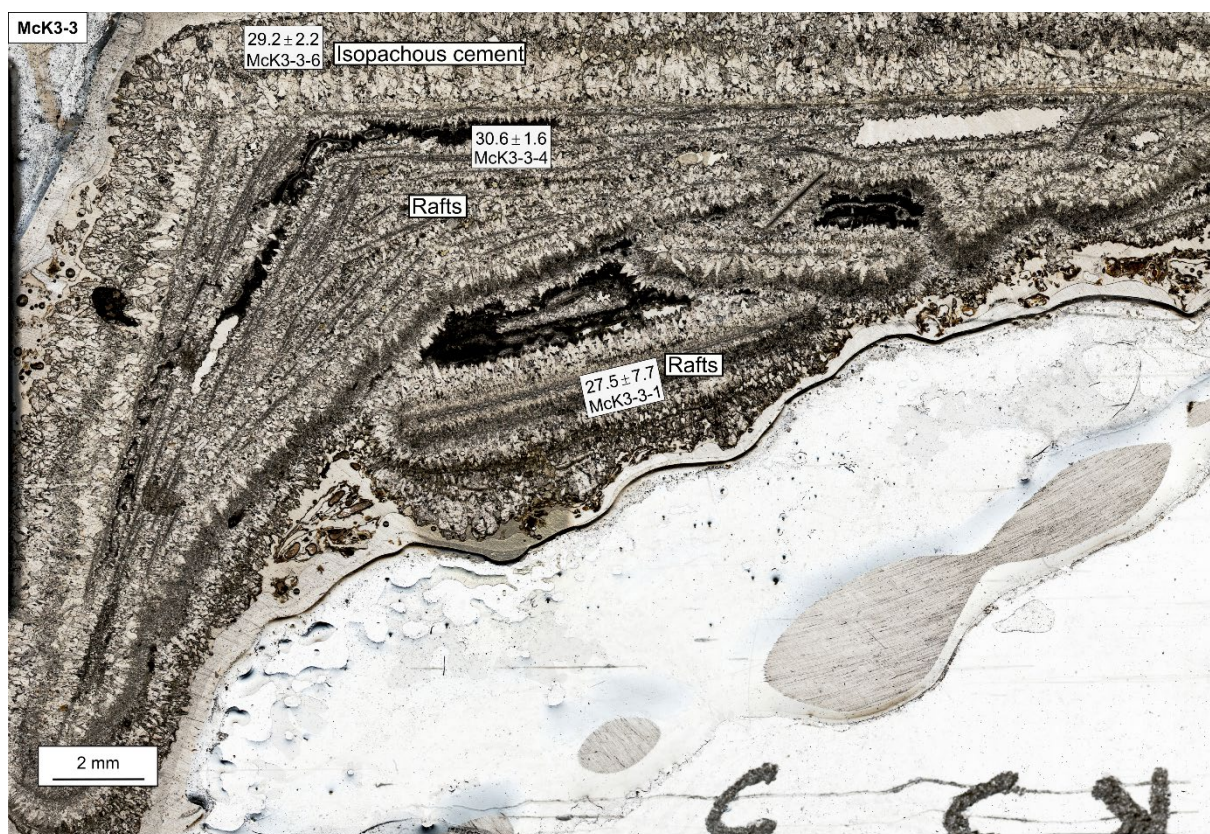


Fig. s10. Thin section of sample McK3-3 with location of U-Pb dated calcite stages (two rafts, McK3-3-1 and 4; one isopachous cement, McK3-3-6).

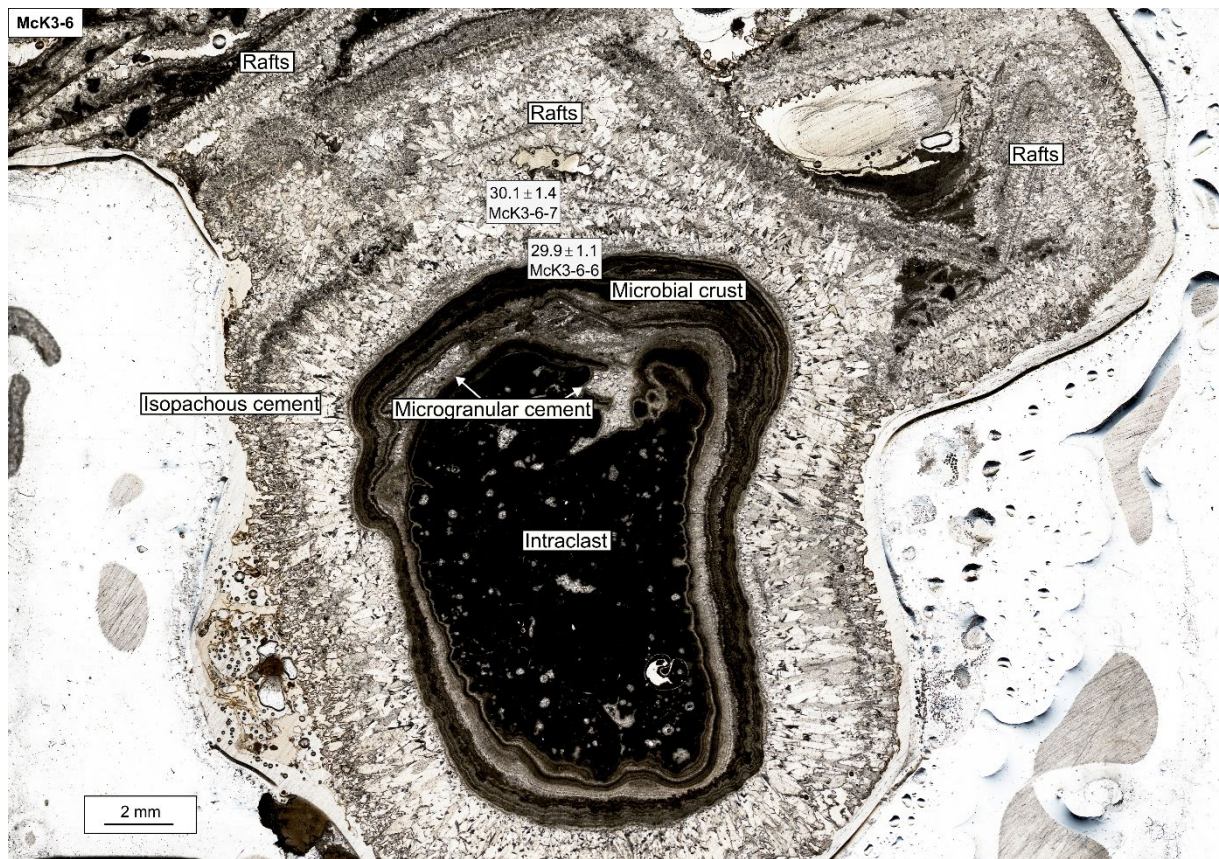


Fig. s11. Thin section of sample McK3-6 with location of U-Pb dated calcite stages (one isopachous cement, McK3-6-6, one raft, McK3-6-7).

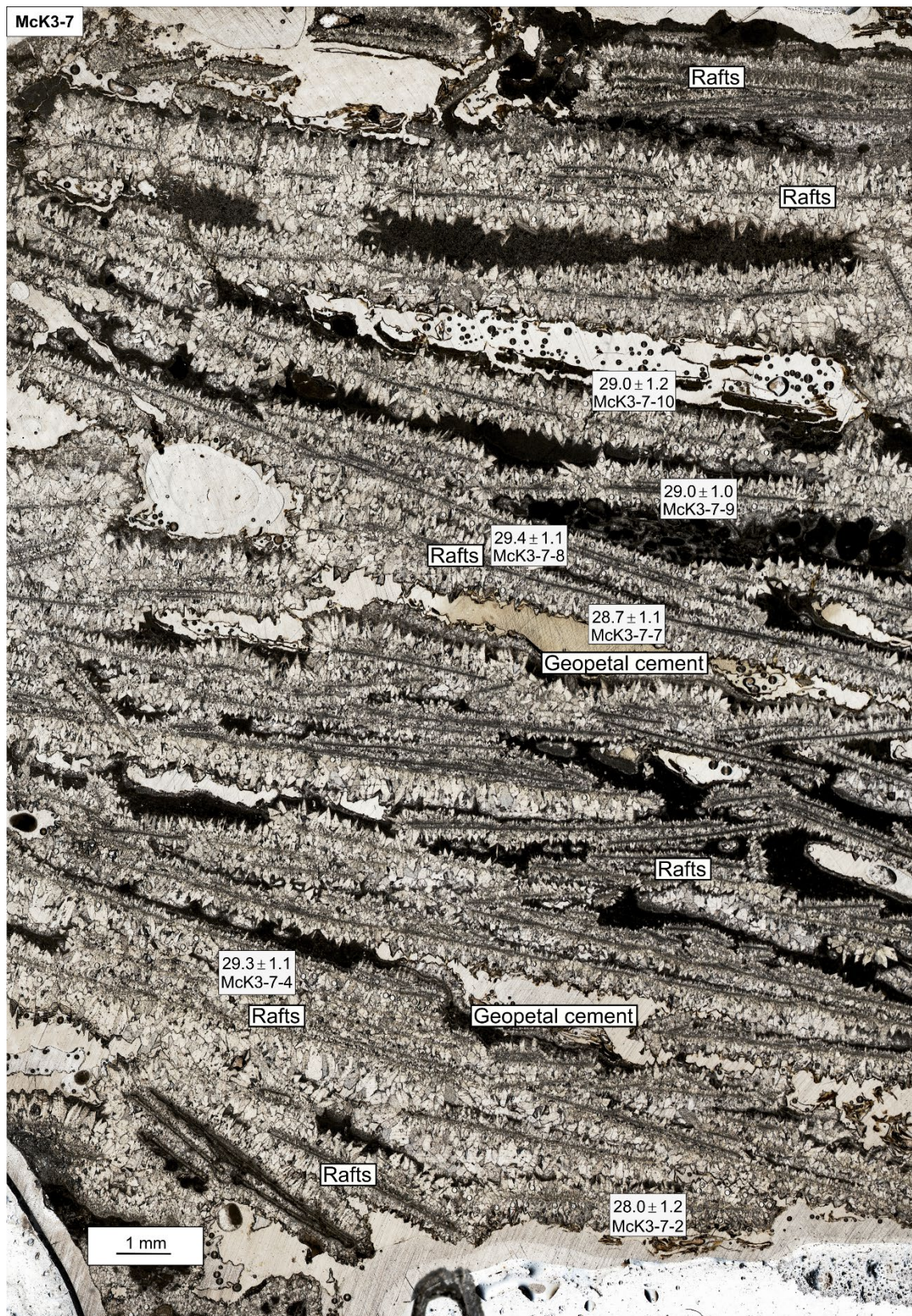


Fig. s12. Thin section of sample McK3-7 with location of U-Pb dated calcite stages (six rafts).

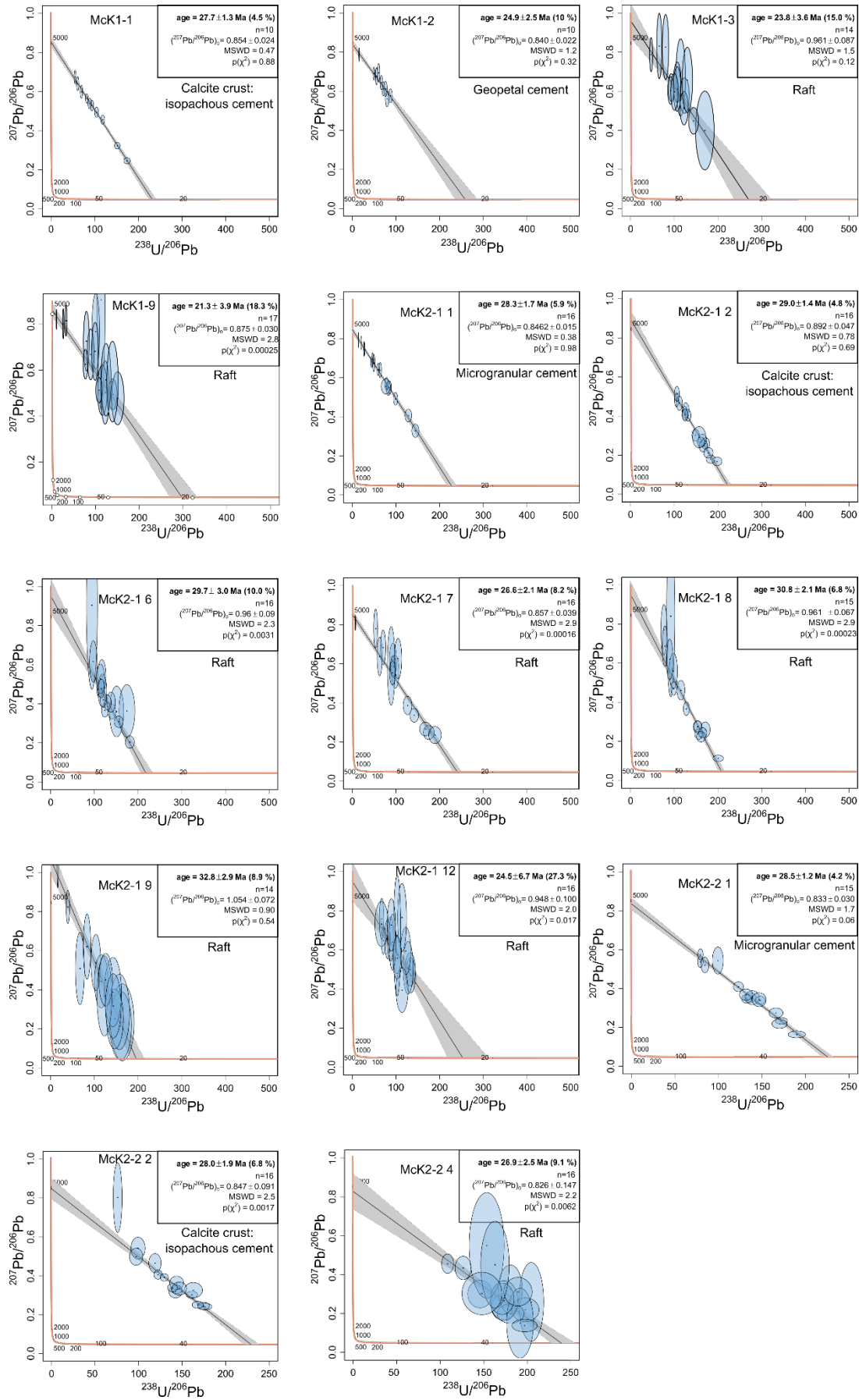


Fig. s13. Tera-Wasserburg diagrams for all the cements dated.

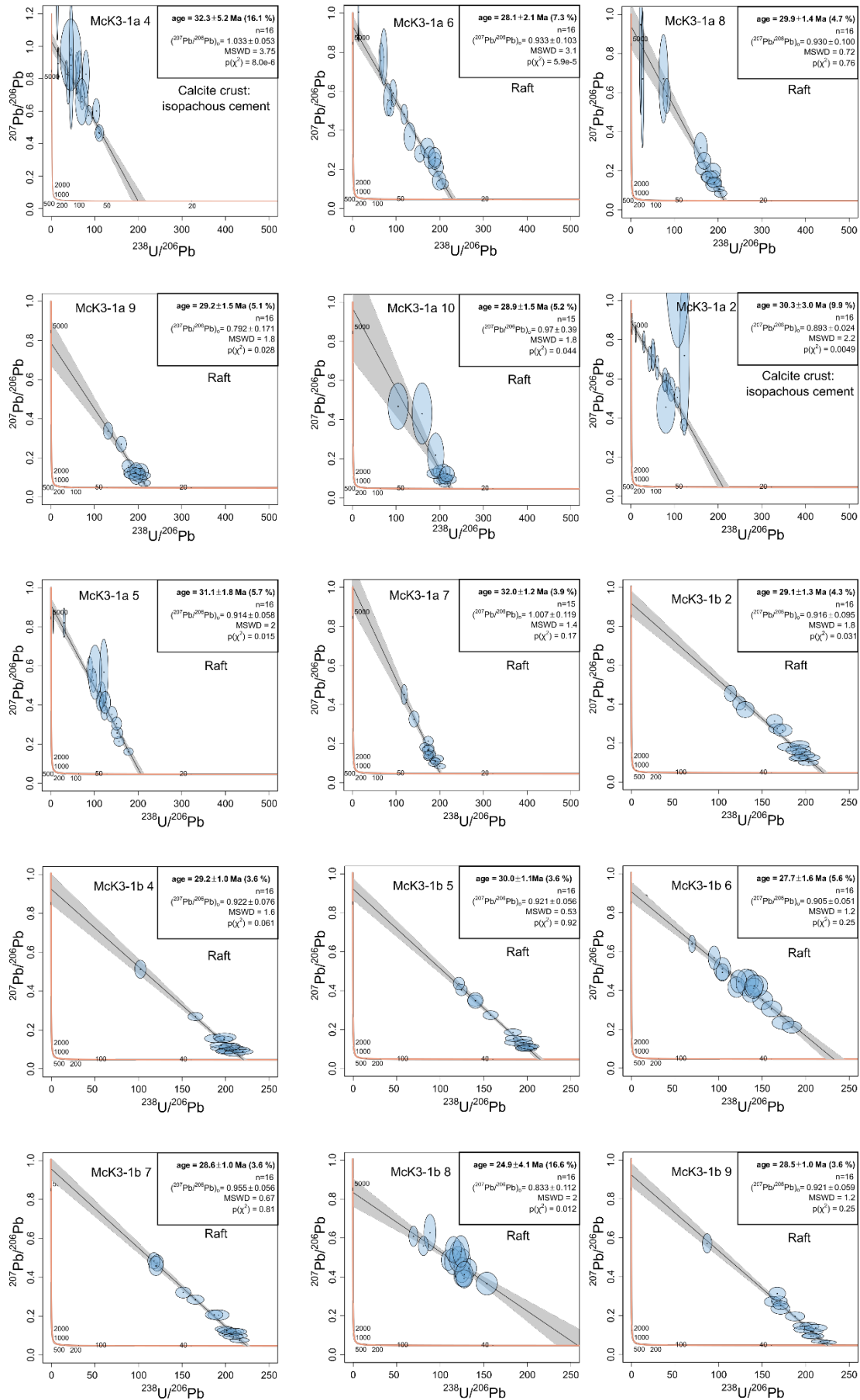


Fig. s13. Tera-Wasserburg diagrams for all the cements dated (continued 1).

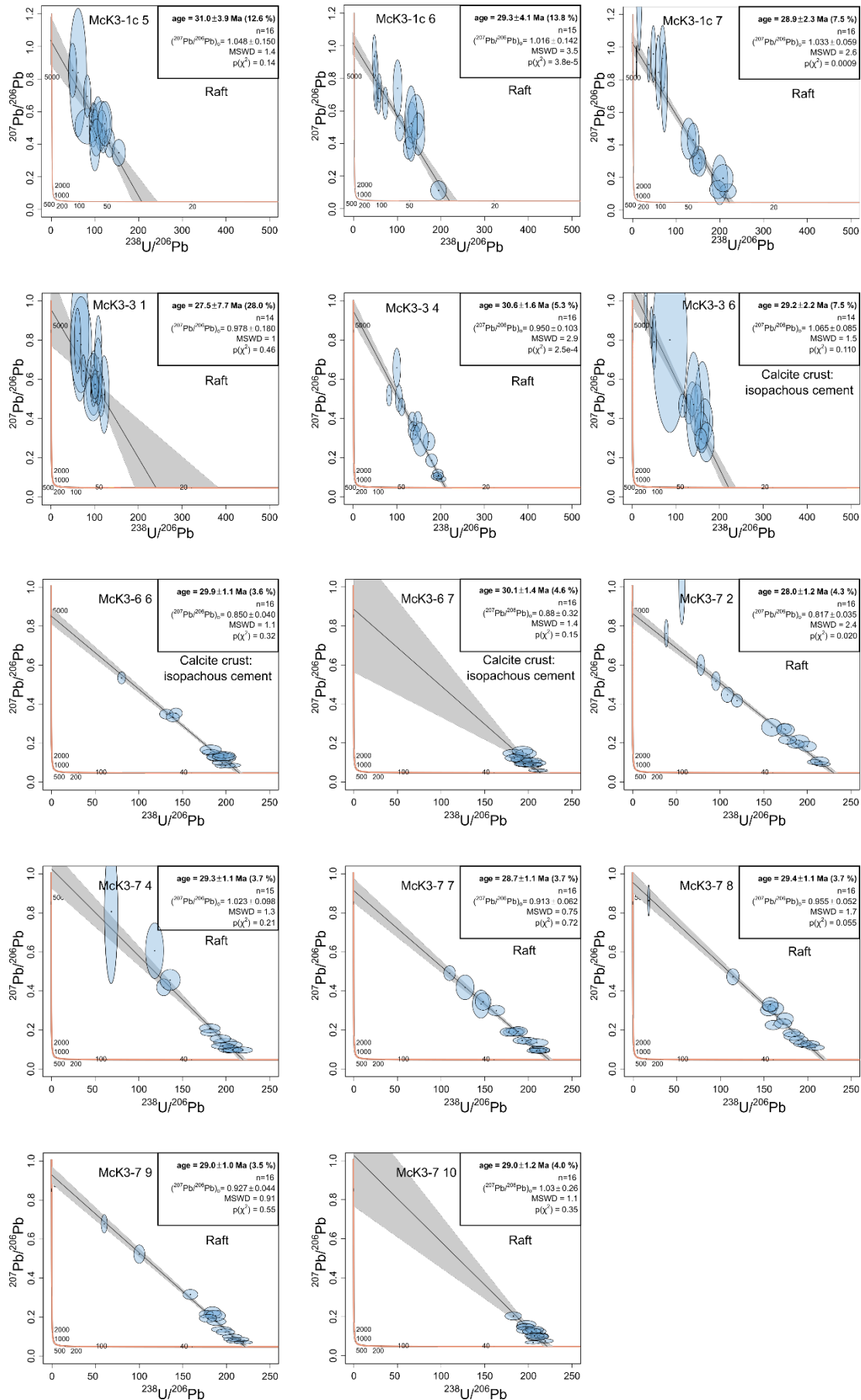


Fig. s13. Tera-Wasserburg diagrams for all the cements dated (continued 2).

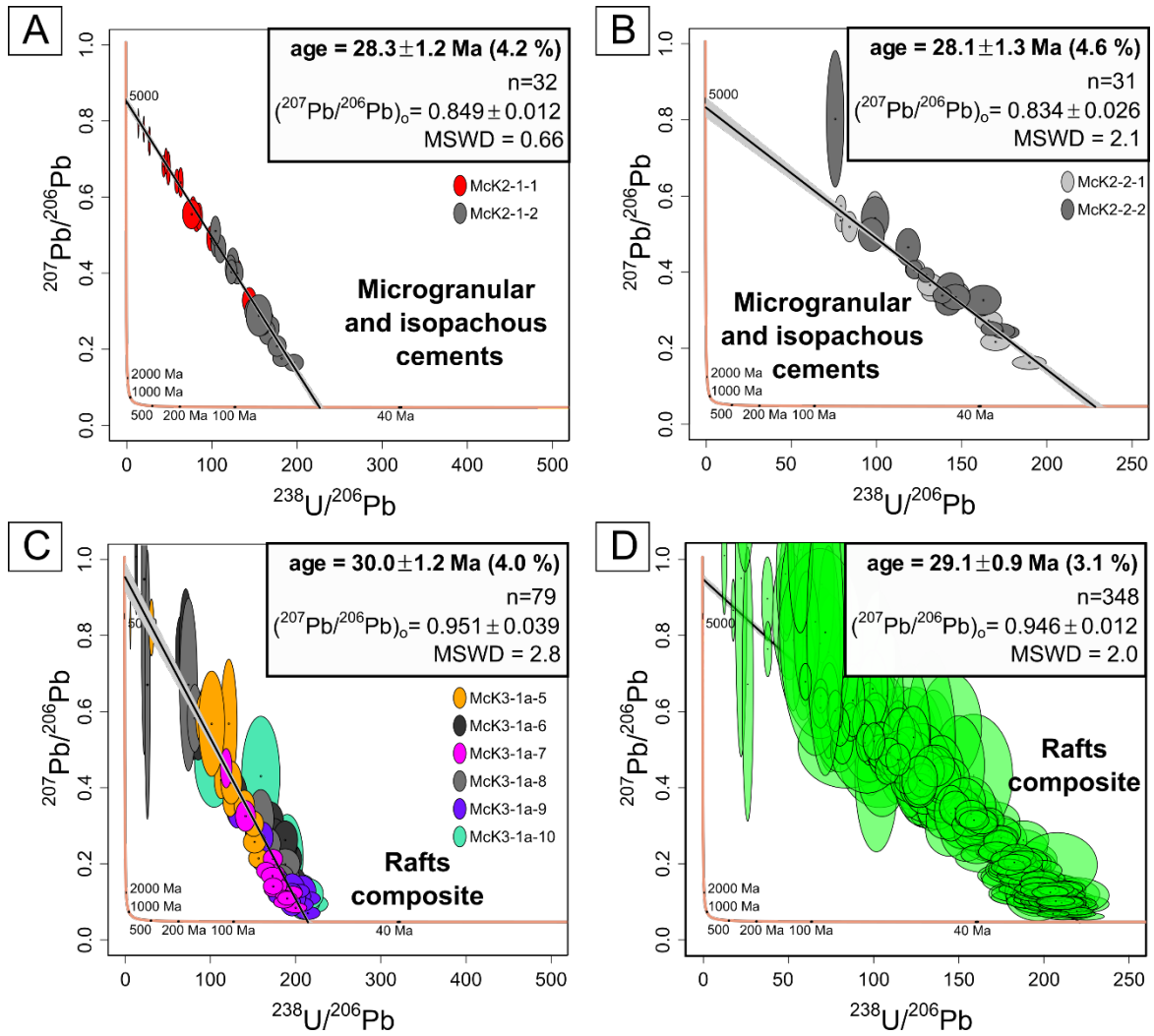


Fig. s14. Tera-Wasserburg diagram combining data from microgranular and isopachous cements in samples McK2-1 (Fig s4; A) and McK2-2 (Fig s5; B), from calcite rafts in McK3-1a (Fig s7; C) whose cements are petrographically individually close to each other and all samples of the McK3 cavity (Fig s6; D).

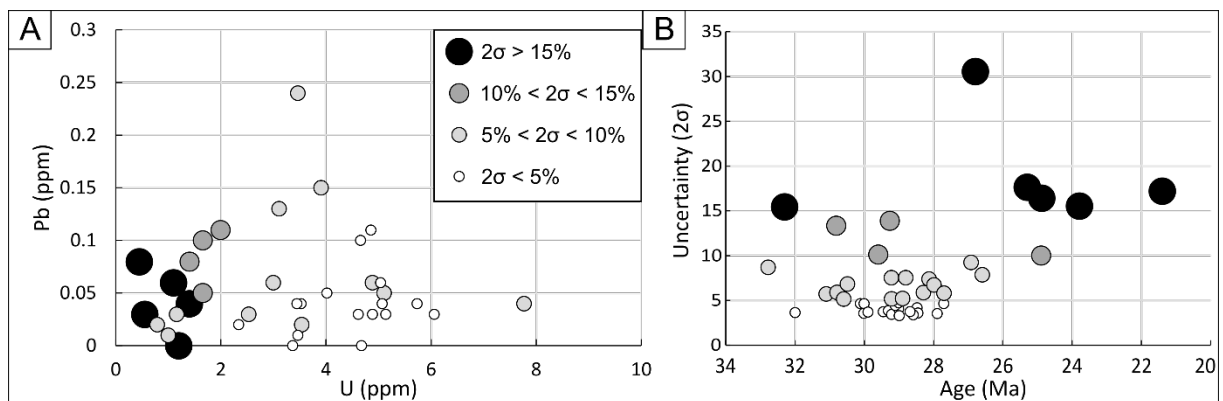


Fig. s15. Diagrams relating the uncertainties (in %) on the U-Pb ages with the U and Pb contents and the ages. Note that the greatest uncertainties are obtained for the youngest calcites containing less than 2 ppm U.

SUPPLEMENTARY REFERENCES LIST

Brigaud, B., Andrieu, S., Blaise, T., Haurine, F., Barbarand, J., 2021. Calcite uranium–lead geochronology applied to hardground lithification and sequence boundary dating. *Sedimentology* 68, 168–195. <https://doi.org/10.1111/sed.12795>

Decker, D.D., Polyak, V.J., Asmerom, Y., Lachniet, M.S., 2018. U-Pb Dating of Cave Spar: A New Shallow Crust Landscape Evolution Tool: U-Pb Dating of Cave Spar. *Tectonics* 37, 208–223. <https://doi.org/10.1002/2017TC004675>

Dunham, R.J., 1962. Classification of carbonate rocks according to depositional textures.

Embry, A.F., Klován, J.E., 1971. A late Devonian reef tract on northeastern Banks Island, NWT. *Bull. Can. Pet. Geol.* 19, 730–781.

Hill, C.A., Polyak, V.J., Asmerom, Y., P. Provencio, P., 2016. Constraints on a Late Cretaceous uplift, denudation, and incision of the Grand Canyon region, southwestern Colorado Plateau, USA, from U-Pb dating of lacustrine limestone. *Tectonics* 35, 896–906. <https://doi.org/10.1002/2016TC004166>

Jochum, K.P., Weis, U., Stoll, B., Kuzmin, D., Yang, Q., Raczek, I., Jacob, D.E., Stracke, A., Birbaum, K., Frick, D.A., Günther, D., Enzweiler, J., 2011. Determination of Reference Values for NIST SRM 610–617 Glasses Following ISO Guidelines. *Geostand. Geoanalytical Res.* 35, 397–429. <https://doi.org/10.1111/j.1751-908X.2011.00120.x>

Lawson, M., Shenton, B.J., Stolper, D.A., Eiler, J.M., Rasbury, E.T., Becker, T.P., Phillips-Lander, C.M., Buono, A.S., Becker, S.P., Pottorf, R., Gray, G.G., Yurewicz, D., Gournay, J., 2018. Deciphering the diagenetic history of the El Abra Formation of eastern Mexico using reordered clumped isotope temperatures and U-Pb dating. *GSA Bull.* 130, 617–629. <https://doi.org/10.1130/B31656.1>

Nuriel, P., Weinberger, R., Kylander-Clark, A.R.C., Hacker, B.R., Craddock, J.P., 2017. The onset of the Dead Sea transform based on calcite age-strain analyses. *Geology* 45, 587–590. <https://doi.org/10.1130/G38903.1>

Pagel, M., Bonifacie, M., Schneider, D.A., Gautheron, C., Brigaud, B., Calmels, D., Cros, A., Saint-Bezar, B., Landrein, P., Sutcliffe, C., Davis, D., Chaduteau, C., 2018. Improving paleohydrological and

diagenetic reconstructions in calcite veins and breccia of a sedimentary basin by combining $\Delta 47$ temperature, $\delta 18\text{O}$ water and U-Pb age. *Chem. Geol.* 481, 1–17.

<https://doi.org/10.1016/j.chemgeo.2017.12.026>

Paton, C., Hellstrom, J., Paul, B., Woodhead, J., Hergt, J., 2011. *Iolite*: Freeware for the visualisation and processing of mass spectrometric data. *J. Anal. At. Spectrom.* 26, 2508–2518.

<https://doi.org/10.1039/C1JA10172B>

Pollard, T., Woodhead, J., Hellstrom, J., Engel, J., Powell, R., Drysdale, R., 2023. DQPB: software for calculating disequilibrium U-Pb ages. *Geochronology*, 5, 181-196.

Roberts, N.M.W., Rasbury, E.T., Parrish, R.R., Smith, C.J., Horstwood, M.S.A., Condon, D.J., 2017. A calcite reference material for LA-ICP-MS U-Pb geochronology: Calcite RM for LA-ICP-MS U-Pb dating. *Geochem. Geophys. Geosystems* 18, 2807–2814. <https://doi.org/10.1002/2016GC006784>

Vennin, E., Bouton, A., Roche, A., Gérard, E., Bundeleve, I., Boussagol, P., Wattinne, A., Kolodka, C., Gaucher, E., Virgone, A., Visscher, P.T., 2021. The Limagne Basin: a journey through modern and fossil microbial deposits☆. *Bull. Société Géologique Fr.* 192, 41.

<https://doi.org/10.1051/bsgf/2021030>

Vermeesch, P., 2018. IsoplotR: A free and open toolbox for geochronology. *Geosci. Front.* 9, 1479–1493. <https://doi.org/10.1016/j.gsf.2018.04.001>

Woodhead, J.D., Hellstrom, J., Maas, R., Drysdale, R., Zanchetta, G., Devine, P and Taylor, E., 2006. U-Pb geochronology of speleothems by MC-ICPMS, *Quaternary Geochronology*, 1, 208-221.

Woodhead, J., Petrus, J., 2020. Exploring the advantages and limitations of in-situ U-Pb carbonate geochronology using speleothems. *Geochronology* 1, 69–84. <https://doi.org/10.5194/gchron-2019-8>